

# Field Effect and Raman Characterization of Self-Assembled MoS<sub>2</sub> Nanoscrolls

Simran Shahi<sup>1</sup>, Maomao Liu<sup>1</sup>, Hemendra Nath Jaiswal<sup>1</sup>, Licheng Xiao<sup>1</sup>, Sichen Wei<sup>2</sup>, Hyun Kim<sup>3</sup>, Seok Joon Yun<sup>3</sup>, Young Hee Lee<sup>3</sup>, Fei Yao<sup>2</sup>, and Huamin Li<sup>1\*</sup>

<sup>1</sup>Department of Electrical Engineering, University at Buffalo, Buffalo, New York, 14260, USA

<sup>2</sup>Department of Materials Design and Innovation, University at Buffalo, Buffalo, New York, 14260, USA

<sup>3</sup>Center for Integrated Nanostructure Physics (CINAP), Institute for Basic Science (IBS), Suwon 16419, Korea

\*Email: [huaminli@buffalo.edu](mailto:huaminli@buffalo.edu) / Phone: (716) 645-1026

Monolayer MoS<sub>2</sub> with a direct and suitable bandgap and high flexibility make them fascinating building blocks for constructing novel nanostructures via a self-assembly process [1, 2]. In this work, we exploit liquid intercalation to activate the self-assembly of MoS<sub>2</sub> nanoscroll (NS) architectures from the monolayer flakes. Both metallic and semiconducting MoS<sub>2</sub> NSs can be identified by field-effect IV characterizations, and further linked to their Raman spectra in a statistical analysis. The self-assembled NS architecture bridges and inherits the unique properties of 1D and 2D nanomaterials, rendering great potential in various applications such as electronic/optoelectronic devices and energy storage.

The high-quality, large-domain monolayer MoS<sub>2</sub> triangular flakes were synthesized directly on SiO<sub>2</sub>/Si substrates using a two-zone chemical vapor deposition (CVD) method [3]. A drop of ethanol solution (volume ratio of ethanol to DI water is 2:1) was applied to the sample, which can relieve the stress in the MoS<sub>2</sub> flakes induced during the synthesis at high temperature and cause them to roll up to form the NS structures [1], as shown in Fig. 1 (a) and (b). The field-effect transistors (FETs) were fabricated using electron beam lithography and evaporation (10 nm Ti and 100 nm Au). The average width and height of the MoS<sub>2</sub> NSs are around 500 and 30 nm, respectively, as confirmed by scanning electron microscopy (SEM) and atomic force microscopy (AFM). Totally 10 MoS<sub>2</sub> NS FETs have been made with the same channel length (1 μm), in a comparison with 3 monolayer MoS<sub>2</sub> planar FETs as the controlling devices, as shown in Fig. 1 (c-e).

Based on the field-effect IV characteristics, the MoS<sub>2</sub> NSs can be classified into two types: metallic (or heavily n-doped) NS and semiconducting NS, as shown in Fig. 2. In the  $J_D$ - $V_G$  transfer characteristics, the metallic NS FETs have a weak gate-modulation and the off-current densities are around 0.001-0.1 μA/μm. Whereas the semiconducting NS FETs have a comparable transistor performance to the planar FETs, including on/off ratio (over 4 orders of magnitude) and on-current densities (around 1 μA/μm). Both the  $J_D$ - $V_D$  output characteristics of the metallic and semiconducting NS FETs show linear IV relations at small drain voltages, indicating good metal-semiconductor contacts for the NS structure. A statistical analysis of transistor performance was carried out, including on/off ratio, electron mobility, maximum on-current density, and subthreshold swing (SS), as shown in Fig. 3. In average, the MoS<sub>2</sub> planar FETs still hold the highest on/off ratio (up to  $10^7$ ) and the lowest SS (0.9 V/dec for 300-nm-thick SiO<sub>2</sub> layer), due to the favorable electrostatic structure. Whereas the semiconducting NS FETs show the improved electron mobility (up to  $12 \text{ cm}^2 \text{ V}^{-1} \text{ s}^{-1}$ ) and on-current density (up to 1.3 μA/μm) which are 3 times higher than the planar FETs. To better understand the performance variation with the formation of MoS<sub>2</sub> NS structure and non-invasively distinguish the metallic and semiconducting NSs, we performed Raman characterization statistically, as shown in Fig. 4. Both the metallic and semiconducting NSs show a blue shift in the A<sub>1g</sub> peak caused by the van der Waals (vdW) interaction with the neighboring layers, and a red shift in the E<sup>1</sup><sub>2g</sub> peak caused by long range Columbic interactions [4]. This is consistent with the NS architecture in which the layers are stacked in an intimate contact with each other. The metallic and semiconducting NSs can be further distinguished by the frequency difference between the A<sub>1g</sub> and E<sup>1</sup><sub>2g</sub> peaks. The metallic NSs has relatively large frequency difference (~25 cm<sup>-1</sup>), compared to the semiconducting NSs (~24 cm<sup>-1</sup>) and the planar MoS<sub>2</sub> (~17.5 cm<sup>-1</sup>). As the planar MoS<sub>2</sub> transforms to the NS structure, the changes of the electronic and photonic properties can be attributed to (i) the uniaxial tensile strain caused by the curved surface of the NS architecture, which alters the electronic band structure accordingly [5], and (ii) the interlayer coupling effect induced in the restacked multilayer structure through vdw interactions.

In summary, the self-assembled MoS<sub>2</sub> NS structures have been investigated using both the electrical and optical characterization methods. The metallic and semiconducting MoS<sub>2</sub> NSs were distinguished from their Raman spectra, and their transistor performance were evaluated statistically in a comparison with the planar MoS<sub>2</sub>.

## References

- [1] X. Cui et al., *Nat. Commun.*, 9, 1301 (2018). [2] Z. Lai et al., *Chem.*, 1, 59 (2016). [3] H. Kim et al., *Nanotech.*, 28, 36 (2017). [4] H. Li et al., *Adv. Funct. Mater.*, 22, 1385 (2012). [5] E. Scalise et al., *Nano Res.*, 5, 43 (2012).

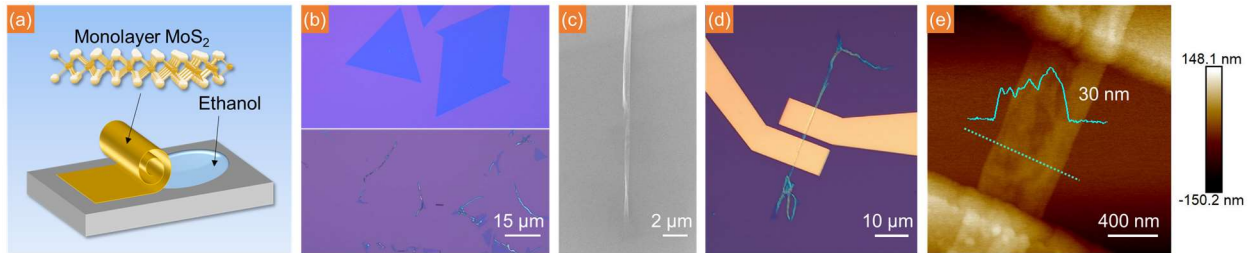


Fig. 1(a) Schematic of MoS<sub>2</sub> NS formation. (b) Optical microscopy images of the as-grown monolayer MoS<sub>2</sub> flakes (top) and the MoS<sub>2</sub> NSs after liquid intercalation (bottom). (c) SEM image of a single MoS<sub>2</sub> NS. (d, e) Optical microscopy image of a MoS<sub>2</sub> NS FET and the corresponding AFM mapping image with the NS height profile.

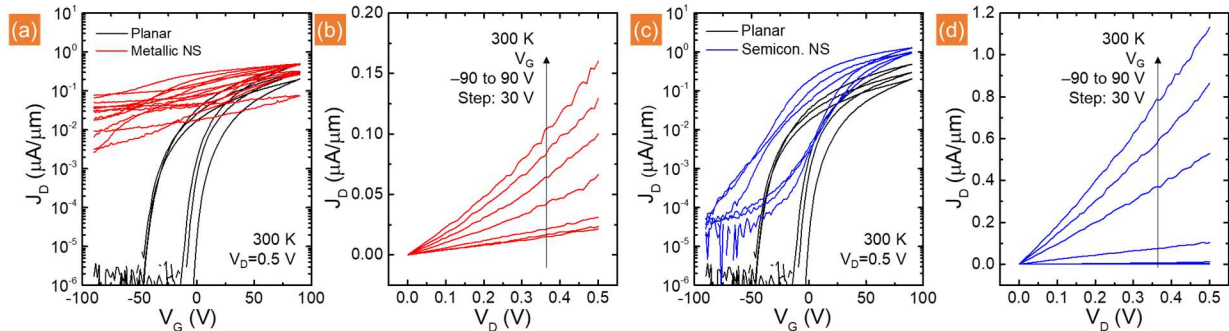


Fig. 2. (a)  $J_D$ - $V_G$  characteristics of totally seven metallic MoS<sub>2</sub> NS FETs at room temperature, in a comparison with three MoS<sub>2</sub> planar FET. (b)  $J_D$ - $V_D$  characteristics of one selected metallic MoS<sub>2</sub> NS FET. (c)  $J_D$ - $V_G$  characteristics of totally three semiconducting MoS<sub>2</sub> NS FETs at room temperature, in a comparison with three MoS<sub>2</sub> planar FET. (d)  $J_D$ - $V_D$  characteristics of one selected semiconducting MoS<sub>2</sub> NS FET.

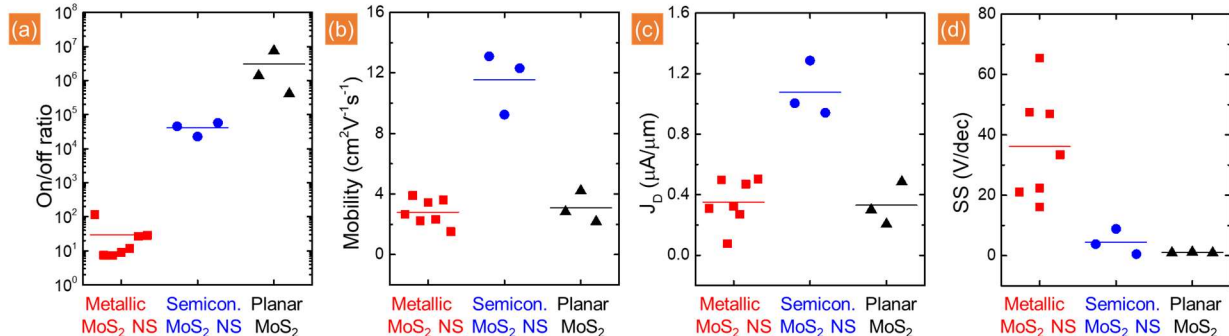


Fig. 3. Statistical analysis of the transistor performance among metallic NS, semiconducting NS, and planar MoS<sub>2</sub> FETs, including (a) on/off ratio, (b) electron mobility, (c) maximum on-current density, and (d) subthreshold swing.

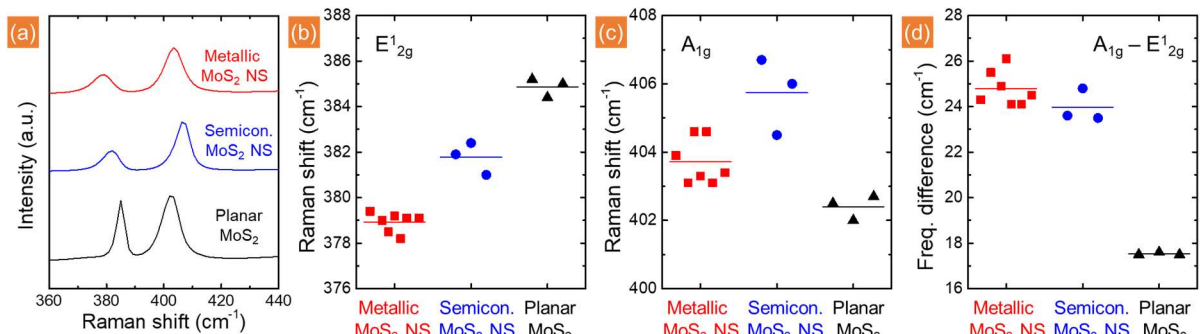


Fig. 4. (a) Comparison of Raman spectra among metallic NS, semiconducting NS, and planar MoS<sub>2</sub> flakes. (b, c, d) Statistical analysis of Raman spectra, including E<sub>1g</sub><sup>2g</sup> peaks, A<sub>1g</sub> peaks, and their frequency difference.